RSC Advances

ROYAL SOCIETY OF CHEMISTRY

www.rsc.org/advances

Synthesis, crystal structure and photoluminescence properties of Eu^{2+}-activated $RbCaGd(PO_4)_2$ phosphors

Xue Chen[a], Qidi Wang[b], Fengzhu Lv[a]*, Paul K. Chu[c], Yihe Zhang[a]*

[a] Beijing Key Laboratory of Materials Utilization of Nonmetallic Minerals and Solid Wastes, National Laboratory of Mineral Materials, School of Materials Science and Technology, China University of Geosciences, Beijing, 100083, China

[b] School of Earth Sciences and Resources, China University of Geosciences, Beijing, 100083, China

[c] Department of Physics & Materials Science, City University of Hong Kong, Tat Chee Avenue, Kowloon, Hong Kong, China

* Corresponding authors: F. Z. Lv: lfz619@cugb.edu.cn; Y. H. Zhang: zyh@cugb.edu.cn; Tel. +86-10-82322759; Fax: +86-10-82322345; Their address is No. 29 Xueyuan Road, Haidian District, Beijing 100083, China.

Abstract

A series of novel double-phosphate compounds $RbCaGd(PO_4)_2:Eu^{2+}$ were first synthesized by the Pechini-type sol-gel method, and their structure and luminescence properties were characterized in detail. The compound $RbCa_{0.97}Gd(PO_4)_2:0.03Eu^{2+}$ crystallizes in the hexagonal system with space group $P6_222$ and the parameters a = 7.006(49) Å, c = 6.358(80) Å, and V = 269.969 Å^3, Z = 1. Its crystal structure is similar to that of hexagonal $LnPO_4$, where the Rb atom occupies a large tunnel in the lattice and the Ln position is statistically occupied by both Gd and Ca(Eu) atoms. In addition, $RbCaGd(PO_4)_2:Eu^{2+}$ produces an intense broadband emission from 400 to 600 nm with the CIE coordinates near (0.2089, 0.2674) and assembles a broad excitation spectrum from 250 to 425 nm. The concentration quenching, crystal field splitting, critical energy transfers distance and thermally stable luminescence properties of $RbCaGd(PO_4)_2:Eu^{2+}$ phosphors are all discussed, which indicate that this material can be considered as a promising bluish green phosphor for application in white-light UV LEDs.

Keywords: Double phosphate; Luminescence properties; $RbCaGd(PO_4)_2$

1. Introduction

Rare-earth doped inorganic phosphors based on their 4*f*-4*f* or 5*d*-4*f* transitions have attracted much attention in displays, optoelectronic devices and white-light-emitting diodes (w-LEDs).[1-3] These materials can produce fluorescent radiation efficiently from ultraviolet (UV) to visible light region with good luminescence yield, which makes them a potential application prospect in solid state lighting region, especially the w-LEDs.[4] Eu^{2+} is a kind of important activator ions for its broad-band emission in white-light-emitting phosphors originating from the $4f^{6}5d$-$4f^{7}$ transition, and it can show a wide range of emissions from blue to red color dependent on the structural characteristics of host crystal.[5-8] Among the various host crystals, the double-phosphate compounds cause extensive concern in many research groups.

Double phosphates, $MNR(PO_4)_2$, where M and N are alkali metal and alkaline earth metal respectively, and R is rare earth element, are isotypic with the corresponding orthophosphates $LaPO_4$ which are well-konwn to exist in three structures viz, hexagonal, monoclinic and tetragonal phases.[9] These phases have several potential applications by doping more different activators for fabrication new compounds because of their environmental friendliness, thermal and chemical stability, and easy synthesis. Hence, lots of studies with double phosphate as host have been performed.[10-14] For example, Et-Tabirou et al[15] reported the structure of $ACaLn(PO_4)_2$ (A = Cs, Rb and K) and confirmed that it was hexagonal $LaPO_4$ type in 1980. Vlasse et al[16] determined the structure of $KCaNd(PO_4)_2$ which was similar to that of hexagonal $LnPO_4$ where the Nd and Ca atoms occupied the Ln position and K atom

occupied a large tunnel. Shaolong Tie et al[17] first reported the optical properties of Ln^{3+} ions (Ln = Gd, Eu and Dy) doped hexagonal $KCaR(PO_4)_2$ (R = Gd, Y) system with no striking concentration quenching for Eu^{3+} and Gd^{3+} activators. Yen-Chi Chen et al[18] reported the $KCaGd(PO_4)_2:Eu^{3+}$ phosphor as a down-converting phosphor to improve the power conversion efficiency of single crystalline silicon-based photovoltaic cells. Dongling Geng et al[19] investigated the optical properties of green/green-yellow-emitting $KSrGd(PO_4)_2:Ce^{3+}$, Tb^{3+}/Mn^{2+} phosphors with high quantum efficiency. Kang Geng et al[20] presented a novel blue-emitting double-phosphate phosphor $Cs_{0.72}Ca_{0.72}Gd_{1.28}(PO_4)_2:Eu^{2+}$ which could be excited by UV light.

To the best of our knowledge, there is no report on the crystal structure and fluorescence properties of the novel double-phosphate compound $RbCaGd(PO_4)_2$. $RbCaGd(PO_4)_2$ crystallizes in the hexagonal system with space group $P6_222$ under ambient conditions. Therefore, Eu^{2+}-doped single-phase $RbCaGd(PO_4)_2$ are prepared by the Pechini-type sol-gel technique in this work. Crystal structure, crystallographic occupancy of Eu^{2+} in $RbCaGd(PO_4)_2$ matrix and their luminescence properties are investigated systematically, which indicates that the novel $RbCaGd(PO_4)_2:Eu^{2+}$ phosphors can act as potential phosphors for application in w-LEDs.

2. Experimental

2.1 Materials and synthesis.

The $RbCaGd(PO_4)_2:Eu^{2+}$ samples were prepared by the Pechini-type sol-gel technique using the following starting materials: $Ca(NO_3)_2 \cdot 4H_2O$ (A.R.), Rb_2CO_3

(A.R.), Gd_2O_3 (99.99%), Eu_2O_3 (99.99%), $(NH_4)_2HPO_4$ (A.R.) and $C_6H_8O_7$ (A.R.) from Beijing Haidian chemical reagent company store. Stoichiometric amounts of Gd_2O_3 and Eu_2O_3 were respectively dissolved in HNO_3 to obtain $Gd(NO_3)_3$ and $Eu(NO_3)_3$ solutions. The detailed synthesis process for $RbCa_{1-x}Gd(PO_4)_2$:xEu^{2+} where x indicates the content of Eu^{2+} was as follows. $Ca(NO_3)_2 \cdot 4H_2O$ and Rb_2CO_3 were dissolved in distilled water under stirring and the predetermined amounts of $Gd(NO_3)_3$, $Eu(NO_3)_3$, $(NH_4)_2HPO_4$ and the citric acid (citric acid/metal ion = 2:1 in mole) were added successively into the above solution and stirred at 80 °C for 30 min until homogeneous gels formed. After drying at 120 °C for 12 h in an oven, the precursor was ground, heated to 500 °C for 10 h in air, ground again, and calcinated at 1100 °C in air for 5 h in CO reducing atmosphere.

2.2 Measurements and Characterization.

The phase identification of the as-prepared samples was carried out on the SHIMADZU model XRD-6000 diffractometer at 40 kV and 30 mA and using monochromatic Cu K_α (λ = 0.15406 nm) radiation. The continuous scanning rate (2θ ranging from 10° to 70°) used for phase identification was 4°(2θ)/min and the data for the Rietveld analysis were collected in a stepping mode with a step size of 0.02° and 8 s/step over the 2θ range from 10° to 120°. The diffraction patterns were analyzed by the General Structure Analysis System (GSAS). The Fourier transform infrared (FT-IR) measurements were performed on a Spectrum One Paragon 1000PC spectrometer over the 1500-400 cm^{-1} region using KBr pellet as backgroud. The room-temperature excitation and emission spectra were recorded on a HITACHI

F-4600 fluorescence spectrophotometer with a photomultiplier at 400 V and 150 W Xe lamp as the excitation lamp. And the temperature-dependent luminescence properties were performed by the same spectrophotometer, which was equipped with a self-made heating apparatus and a computer controlled electric furnace. The luminescence decay curve was obtained from a lifetime and steady state spectrometer (Edinburgh Instruments Ltd, FLS920) with a 335 nm pulse laser radiation (nano-LED) as the excitation source. The quantum efficiency was measured on an absolute photoluminescence quantum yield measurement system (Nanolog^{R} FluoroLog-3-2-iHR320, Horiba Jobin Yvon) with F-3018 integral sphere.

3. Results and discussion

3.1 Phase analysis.

The XRD patterns of the synthesized $RbCaGd(PO_4)_2:Eu^{2+}$ phosphors and the Joint Committee on Powder Diffraction Standards (JCPDS) reference card of $RbCaGd(PO_4)_2$ are depicted in Figure 1 (a). The diffraction patterns of the synthesized samples can be indexed to the standard card of $RbCaGd(PO_4)_2$ (JCPDS, No. 34-0091), which is a hexagonal phase with the space group of *P6$_2$22*. No other peaks are observed indicating complete dissolution of the dopants in the $RbCaGd(PO_4)_2$ host and no significant changes in the crystal structure.

For the first time, the crystal structure of $RbCaGd(PO_4)_2$ was determined. The crystal structure of double phosphate of $RbCa_{0.97}Gd(PO_4)_2:0.03Eu^{2+}$ host lattice is refined using the computer software GSAS. The Rietveld structure of the

$RbCa_{0.97}Gd(PO_4)_2$:$0.03Eu^{2+}$ and the single crystal data of the ICSD-35098-$KCaNd(PO_4)_2$ phase model are shown in Figure 1(b). No impurity phase is detected and the fractional atomic coordinates, occupancy, and isotropic thermal parameters of $RbCa_{0.97}Gd(PO_4)_2$:$0.03Eu^{2+}$ are presented in Table 1. Rb^+ and Gd^{3+} are designed to occupy the sites of K^+ and Nd^{3+}, respectively, due to the similar ion radius and equal valence. Table 1 also lists the reflection conditions R_{wp}(%) = 8.62, *Rp(%)* = 6.34 and χ^2= 2.01. The parameters suggest that pure $RbCaGd(PO_4)_2$:$0.03Eu^{2+}$ is synthetized and indexed to the hexagonal crystal system and space group $P6_222$, a = 7.006(49) Å, c = 6.358(80) Å, and V = 269.969 $Å^3$. The schematic illustration of the crystal structure of $RbCaGd(PO_4)_2$ viewed from the c axis and the coordination environment around Rb^+ and Ca^{2+}/Gd^{3+} are shown in Figure 1 (c). Rb^+ is coordinated by 8O located along the c axis whereas Ca^{2+}/Gd^{3+} is coordinated to 8O with the distorted D_2 point symmetry forming the chains of –(Ca^{2+}/Gd^{3+})–(PO_4)–(Ca^{2+}/Gd^{3+})– running along the *c*-axis which forms the edge sharing [Ca/GdO_8] polyhedra chains interconnected by corner sharing. These interconnected chains leave large open channels, which is occupyied by Rb atom with oxygen lined tunnels parallel to the c axis.

The FT-IR spectra of the double phosphates are shown in Figure 2 (a). Due to small amounts of the dopant ions, the spectra of the doped and undoped samples are similar, therefore only one representative spectrum for $RbCaGd(PO_4)_2$:Eu^{2+} is shown in this figure. The singlet strong absorption band centered at 1074 cm^{-1} attributes to the asymmetric stretching of PO_4 groups, while the symmetric stretching of the same

groups manifests at the 1001 cm^{-1}. Two bands centered at 609 and 503 cm^{-1} are due to the asymmetric deformation modes of PO_4 groups, and a single band centered at 414 cm^{-1} is due to symmetric deformation modes of PO_4 groups. The FT-IR results show that all vibrations originate from the anion groups of PO_4 units, and one of the characteristic feature of the phosphates is the low number of absorption bands. Some similar results have been observed in the other types of hexagonal phosphates.[21-22]

3.2 Photoluminescence properties of the $RbCaGd(PO_4)_2:Eu^{2+}$ phospors.

The PLE and PL spectra of the $RbCaGd(PO_4)_2:0.03Eu^{2+}$ are displayed in Figure 2 (b). The PLE spectrum monitored at 476 nm exhibits two obvious bands from 250 to 425 nm, which originate from the electron transition from the ground state $4f^7$ to the crystal-field split $4f^65d$ levels of Eu^{2+} in the host lattice. Upon excitation at 334 nm, all of the emission spectra of $RbCaGd(PO_4)_2$: xEu^{2+} show a similar board band from 435 to 600 nm peaking at 476 nm attributable to the transitions between the 5d excited state and 4f ground state. In order to further understand the origin of the emission centered at 476 nm, the experiential equation of Van Uitert is adopted to fit the emission peak and excitation edge data[23] and the crystallographic site substituted by Eu^{2+} in $RbCaGd(PO_4)_2$ is investigated theoretically:

$$E = Q\left[1-\left(\frac{V}{4}\right)^{\frac{1}{V}} 10^{-\frac{n\times Ea\times r}{80}}\right] \quad (1)$$

where E is the energy of the d-band edge for rare earth ions (cm^{-1}) equivalent to the wavelength of 470 nm, V is the valence of the activator (Eu^{2+}) with V = 2, Q represents the energy of the lower d-band edge of the free ions (34,000 cm^{-1} for Eu^{2+}),

n is the coordination number of the "active" ion (Eu^{2+}), *r* is the effective radius of the host replaced by the "active" ion, *Ea* is the constant electron affinity of the atoms that form anions in the same host. Here, *Ea* is 2.5 eV as reported from other phosphate systems and as discussed above, Eu^{2+} occupies the Ca^{2+} site in the $RbCaGd(PO_4)_2$ host and the effective ionic radii of Ca^{2+} is 1.12 Å. The calculated *n* is 7.9 which means that Eu^{2+} has eight coordination elements.

The PL spectra of the $RbCaGd(PO_4)_2$:*x*Eu^{2+} are displayed in Figure 3 (a). Excited by 334 nm irradiation, all of the emission spectra of $RbCaGd(PO_4)_2$:*x*Eu^{2+} show a similar spectral profiles due to the 4f-5d transition of Eu^{2+}. But the peak red-shifts as the concentration of Eu^{2+} increases gradually. It originates from the change in the crystal field strength as shown in the following:[24]

$$Dq = \frac{ze^2r^4}{6R^5} \quad (2)$$

where *Dq* is the crystal field strength, *e* is the charge of an electron, *r* is the radius of the central ions, *d* is the wave function, *z* is the charge or valence of the anion, and *R* is the bond distance between the central ion and ligands. Based on this equation, a shorter bond length increases the crystal field strength when the crystal environment is homologous. When Ca^{2+} is substituted by the larger Eu^{2+}, the distance between Eu^{2+} and O^{2-} becomes shorter and the crystal field strength increases. As a result, the emission wavelength red-shifts with increasing Eu^{2+} concentrations.

The concentration dependence of the emission intensity of the phosphors on Eu^{2+} is demonstrated in the inset of Figure 3 (a). The PL emission intensity increases, reaches a maximum at the Eu^{2+} concentration of 0.03, and decreases afterwards due to

concentration quenching. Concentration quenching is due to the energy transfer from one activator to another. So it is necessary to calculate the critical transfer distance (R_c) of the activator and quenching site. The optimum Eu^{2+} concentration can be used to determine concentration quenching caused by energy transfer mechanisms such as exchange interaction, radiation reabsorption, or multipole-multipole interaction and R_c can be estimated with geometrical consideration according to the following formula:[25]

$$R_C \approx 2\left[\frac{3V}{4\pi x_c N}\right]^{1/3} \quad (3)$$

where N is the number of host ions in the unit cell, V is the unit cell volume of the unit cell, and x_c is the atom fraction of the activator at which quenching occurs. In the $RbCaGd(PO_4)_2$ host, the crystallographic parameters are $V = 269.980 Å^3$, $N = 1$, and $x_c = 0.03$. According to Equation 3, the critical distance R_c is determined to be 28.81 Å indicating that the nonradiative concentration quenching takes place among two nearest Eu^{2+} via electric multipolar interactions based on the Dexter theory. In order to further investigate the energy transfer mechanism, the interaction type between the sensitizers or between the sensitizer and activator is confirmed by equation 4:[26]

$$I/x = k\left[1+\beta(x)^{\theta/3}\right]^{-1} \quad (4)$$

In this equation, I is the emission intensity, x is the activator concentration which is not less than the critical concentration, k and β are constants under the same excitation conditions for a given host crystal, and θ = 6, 8, 10 for the dipole-dipole (*d*-*d*), dipole-quadrupole (*d*–*q*), or quadrupole-quadrupole (*q*–*q*) interactions, respectively. To obtain the correct θ, the dependence between log(I/x) and log(x) based on equation 4 is plotted in Figure 3 (b). The slope of the straight line is determined to be -1.78 and

θ is calculated to be 5.34 that is close to 6, indicating that the dipole-dipole interaction is the major concentration quenching mechanism in $RbCaGd(PO_4)_2:Eu^{2+}$.

The temperature dependence of luminescence from the $RbCaGd(PO_4)_2:0.03Eu^{2+}$ phosphor under 334 nm excitation is presented in Figure 3 (c). As the temperature goes from 30 ^oC up to 150 ^oC, the PL intensity diminishes to 37% of the initial value. In general, the configurational coordinate diagram is used to explain thermal luminescence quenching as the excited luminescence center is thermally activated through the crossing point between the ground state and the excited state. This nonradiative transition depends strongly on the temperature resulting in reduction in the emission intensity. When the temperature is increased, the intensity decreases and the full-width at half-maximum (FWHM) increases as described by the Boltzmann distribution function as follows:[27]

$$FWHM(T) = W_0\sqrt{\coth\left(\frac{hw}{2kT}\right)} \quad (5)$$

$$W_0 = \sqrt{8\ln 2}(hw)\sqrt{S} \quad (6)$$

In the above equations, *hw* is the energy of the lattice vibration that interacts with the electronic transition, W_0 is the FWHM at 0 K, *k* is Boltzmann's constant, and *S* is the Huang-Rhys-Pekar parameter showing the strength of the electron-lattice coupling. It is postulated that *hw* is the energy of the vibrational levels of the $4f^7$ ground state or $4f^6 5d$ excited state of Eu^{2+}. As the temperature is increased, the electron-phonon interaction becomes dominant and a higher temperature increases the FWHM of the emission line. The activation energy (E) of thermal quenching can be estimated by the Arrhenius equation:[28]

$$I(T) \approx \frac{I_0}{1 + c\exp(\frac{-E}{kT})} \quad (7)$$

where I_0 is the initial PL intensity of the phosphor, I(T) is the intensity at the given temperature, c is a constant for a certain host, k is Boltzmann's constant (8.62×10^{-5} eV), and E is the activation energy of thermal quenching. Figure 3 (d) plots the relationship of $\ln(I_0/I_T)$-1 vs. $1/k$T, where the straight slope is equal to $-E$ and the activation energy E of $RbCaGd(PO_4)_2$:$0.03Eu^{2+}$ is 0.3117 eV. A red shift behavior is observed as the temperature goes up and it can be explained by the semi-empirical Varshni equation:[29]

$$E(T) = E_0 - \frac{aT^2}{T + b} \quad (8)$$

where E_0 is the energy difference between the excited and ground states at 0 K, $E(T)$ is the energy difference at temperature T, and a and b are fitting parameters. The covalent bond between the luminescent center and ligand ions becomes stronger and the interaction between electrons is reduced due to the expansion of the electron clouds, resulting in the decreased crystal field as the temperature is increased. Moreover, the symmetry of the luminescent center is distorted so that the Jahn-Teller effect is dominant. Splitting of the degenerate excited state or ground state causes these two effects which drive the emission peak shift to lower energies.

Figure 4 presents the decay curves of the Eu^{2+} luminescence in $RbCaGd(PO_4)_2$:Eu^{2+} with different Eu contents (0.1-0.10 mol%) upon excitation at 335 nm. In this work, the decay time of all the samples are characterized by average lifetime (τ^*), which can be calculated based on the following expression:[30]

$$\tau = \frac{\int_0^\infty I(\mathrm{t}) t dt}{\int_0^\infty I(\mathrm{t}) \mathrm{dt}} \quad (9)$$

Where *I(t)* is the luminescence intensity at a time t. According to the equation, the effective lifetime τ^* is determined to be 0.978, 0.927, 0.884, 0.845 and 0.767 μs for $RbCaGd(PO_4)_2$:$x$$Eu^{2+}$ with x = 0.01, 0.03, 0.05, 0.08 and 0.10, respectively. Those results are reasonable for the allowed 5d-4f transition of Eu^{2+} ions, which is known occurring in less than a microsecond. The lifetime for the Eu^{2+} ions decrease monotonically with increasing Eu^{2+} concentration due to the increase of the nonradiative and self-absorption rate of the internal doped ions when activators cross the critical separation between activator ion and quenching site.

The x and y values of CIE chromaticity coordinates for $RbCaGd(PO_4)_2$:$x$$Eu^{2+}$ (x = 0.01, 0.03, 0.05, 0.08 and 0.10) were calculated and presented in Table 2. The results obtained is shown in CIE chromaticity diagram of Figure 5. Besides, the images of phosphors excited by 365 nm are also given in the inset of Figure 5. The emission light can be clearly observed by the naked eye. The chromaticity coordinates for $RbCaGd(PO_4)_2$:$x$$Eu^{2+}$ could be tuned from greenish blue (0.2169, 0.2543) to bluish green (0.2639, 0.3097) position by changing the Eu^{2+} concentration. Additionally, the measured internal quantum efficiency (QE) of $RbCaGd(PO_4)_2$:0.03Eu^{2+} phosphor is determined as 13.32% under 334 nm excitation which is not high enough. But the QE can be improved by adjustment the particle size, morphology, size distribution and crystalline defects through optimization of the processing conditions.

4. Conclusion

In summary, a novel blue-emitting phosphors composed of $RbCaGd(PO_4)_2:Eu^{2+}$ are first reported. The crystal structure of $RbCaGd(PO_4)_2:0.03Eu^{2+}$ matrix is discussed based on Rietveld refinements results. The series of phosphors show a board band at 476 nm due to the 4f-5d transition. The calculated *Rc* for the energy transfer from one Eu^{2+} to another Eu^{2+} in the phosphor, which is electrostatic multipolar interaction, is 28.81 Å. Concentration quenching resulting from the dipole-dipole interaction is observed. With increasing of the Eu^{2+} concentration, the CIE coordinates slightly shift from greenish blue (0.2169, 0.2543) to bluish green (0.2639, 0.3097) position. These results suggest that the $RbCaGd(PO_4)_2:Eu^{2+}$ exhibits a potential application in the solid-state lighting field.

Acknowledgements

The work was jointly supported by the Fundamental Research Funds for the Central Universities (2-9-2013-49) and City University of Hong Kong Strategic Research Grant 7004188 and Guangdong - Hong Kong Technology Cooperation Funding Scheme (TCFS) GHP/015/12SZ.

References

1 H. A. Hoppe, *Angew. Chem. Int. Ed.*, 2009, **48**, 3572.

2 H. H. Nersisyan, H. I. Wona, C. W. Won, A. G. Kirakosyan and D. Y. Jeon, *Chem. Eng. J.*, 2012, **198 (199)**, 449.

3 Z. J. Wang , J. P. Zhong, H. X. Jiang, J. Wang and H. B. Liang, *Cryst. Growth Des.*, 2014, **14**, 3767.

4 Y. F. Pu, H. Weng, H. Cheng, S. I. Kim and H. J. Seo, *J. Lumin.*, 2015, **168**, 77.

5 H. Yu, D. G. Deng, Y. Q. Li, S. Q. Xu, Y. Y. Li, C. P. Yu, Y. Y. Ding, H. W. Lu, H. Y. Yin and Q. L. Nie, *J. Lumi*n., 2013, **143**, 132.

6 S. X. Li, X. Peng, X. J. Liu and Z. R. Huang, *Opt. Mater.*, 2014, **38**, 242.

7 C. H. Huang, D. Y. Wang, Y. C. Chiu, Y. T. Yeh and T. M. Chen, *RSC Adv.*, 2012, **2**, 9130.

8 H. Yu, Yu, D. Deng, L. Chen, D. Chen, J. Zhong, H. Zhao and S. Xu, *Ceram Int*, 2015, **41(3)**, 3800.

9 T. N Sairam, G. V Narasimha Rao and B Viswanathan, *B Mater Sci*, 1999, **22(4)** 751.

10 Z. J. Zhang, J. L. Yuan, S. Chen, H. H. Chen, X. X. Yang, J. T. Zhao, G. B. Zhang, C. S. Shi, *Opt. Mater.* 2008, **30**, 1848.

11 D. L. Geng, M. M. Shang, D. M. Yang, Y. Zhang, Z. Y. Cheng, J. Lin, *J. Mater. Chem.* 2012, **22**, 23789.

12 W. R. Liu, C. H. Huang, C. W. Yeh, J. C. Tsai, Y. C. Chiu, Y. T. Yeh and R. S. Liu, *Inorg. Chem.* 2012, **51**, 9636.

13 W. R. Liu, C. H. Huang, C. W. Yeh, Y. C. Chiu, Y. T. Yeh and R. S. Liu, *RSC Adv.*, 2013, **3**, 9023.

14 W. R. Liu and P. C. Lin, *Opt. Express* 2014, 22(S2), 446.

15 M. Et-Tabirou , A. Daoudi, *C. R. Acad. Sci. Paris*, 1980, **291C**, 93.

16 M. Vlasse, P. Bochu, C. Parent, J. P. Chaminade, A. Daoudi, G. LeFlem and P. Hagenmuller, *Acta Cryst.*, 1982, **B38**, 2328.

17 S. L. Tie, Q. Su and Y. Q. Yu, *Phys. Stat. Sol. (a).*, 1995, *147(1)*, 267.

18 Y. C. Chen, W. Y. Huang and T. M. Chen, *J. Rare Earth.*, 2011, **29(9)**, 907.

19 D. L. Geng, M. M. Shang, D. M. Yang, Y. Zhang, Z. Y. Cheng and J. Lin, *Dalton Trans*, 2012, **41**, 14042.

20 K. Geng, Z. G. Xia and M. S. Molokeev, *Dalton Trans*., 2014, **43**, 14092.

21 P. Godlewska, A. Matraszek, L. Macalik, S. M. Kaczmarek, T. Skibiński, K. Hermanowicz, M. Ptak, R. Lisiecki, W. Ryba-Romanowski, I. Szczygieł and J. Hanuza, *J. Alloy. Compd*, 2014, **606**, 124.

22 P. Godlewska, A. Matraszek, L. Macalik, K. Hermanowicz, M. Ptak, P. E. Tomaszewski, J. Hanuza and I. Szczygieł, *J. Alloy. Compd*, 2015, **628**, 199.

23 L. G. Van Uitert, *J. Lumin.*, 1984, **29(1)**, 1.

24 P. D. Rack and P. H. Holloway, *Mater. Sci. Eng. R.*, 1998, **21**, 171.

25 J. H. Kim and K. Y. Jung, *J. Lumin.*, 2011, *131*, 1487.

26 Z. G. Xia, Y. Y . Zhang, M. S. Molokeev, V. V. Atuchin, *J. Phys. Chem. C.*, 2013, **117(40)**, pp 20847.

27 M. Zhang, J. Wang, Z. Zhang, Q. Zhang and Q. Su, *Appl Phys B.*, 2008, **93**, 829.

28 S. Y. Zhang, Y. Nakai, T Tsuboi, Y. L. Huang and H.J. Seo, *Chem. Mater.*, 2011, **23**, 1216.

29 J. S. Kim, Y. H. Park, S. M. Kim, J. C. Choi and H. L. Park, *Solid State Commun.*, 2005, 133, 445.

30 G. Blasse and B. C. Grabmaier, Luminescent Materials, Springer-Verlag, Berlin, 1994. Z. G. Xia and R. S. Liu, *J. Phys. Chem. C.*, 2012, **116**, 15604.

Table captions

Table 1 Fractional atomic coordinates, occupancy, and isotropic thermal parameters of $RbCaGd(PO_4)_2$ obtained by GSAS Rietveld Refinement using powder X-ray diffraction data at room temperature.

Table 2 CIE chromaticity coordinates of $RbCaGd(PO_4)_2$:$x$$Eu^{2+}$ (x = 0.01, 0.03, 0.05, 0.08 and 0.10) phosphors.

Figure captions

Figure 1 XRD patterns of the as-prepared $RbCaGd(PO_4)_2:Eu^{2+}$ phosphors (a), rietveld structure analysis (b) of the selected $RbCaGd(PO_4)_2:0.03Eu^{2+}$ phosphor and crystal structure (c) of $RbCaGd(PO_4)_2$.

Figure 2 The FT-IR spectrum (a), PL and PLE spectra (b) of the $RbCaGd(PO_4)_2:0.03Eu^{2+}$ phosphor.

Figure 3 PL spectra (a) and relationship (b) of log(x) *vs*. log(I/x) for the $RbCaGd(PO_4)_2:xEu^{2+}$ (x = 0.01, 0.03, 0.05, 0.08 and 0.10) phosphors, emission spectra (c) of $RbCaGd(PO_4)_2:0.03Eu^{2+}$ excitation under 334 nm at different temperature and (d) activation energy of thermal quenching.

Figure 4 Decay curves of Eu^{2+} in $RbCaGd(PO_4)_2:xEu^{2+}$ phosphors (excited at 335 nm, monitored at 467 nm).

Figure 5 CIE chromaticity diagram and the digital photograph for $RbCaGd(PO_4)_2:xEu^{2+}$ (x = 0.01, 0.03, 0.05, 0.08 and 0.10) excited by 365 nm.

Table 1 Fractional atomic coordinates, occupancy, and isotropic thermal parameters of $RbCaGd(PO_4)_2$ obtained by GSAS Rietveld Refinement using powder X-ray diffraction data at room temperature.

Atom	*x*	*y*	*z*	Occupancy	U_{iso}/Å^2	Multiplicity
Rb	0	0	1/2	0.5	0.071(91)	3c
Ca	1/2	0	0	0.483(12)	0.007(97)	3c
Eu	1/2	0	0	0.016(63)	0.007(97)	3b
Gd	1/2	0	0	0.5	0.007(97)	3c
P	1/2	0	1/2	1.0	0.011(79)	3d
O	0.4348(45)	0.1356(84)	0.3529(56)	1.0	0.028 (01)	12k

space group: $P6_222$ - hexagonal; a = 7.006(49) Å, c = 6.358(80) Å, V = 269.969Å^3; α = 90º,γ = 120º; 2θ-interval = 10-120º; R_{wp}*(%)* = 8.62, R_p*(%)* = 6.34, χ^2 = 2.01

Table 2 CIE chromaticity coordinates of $RbCaGd(PO_4)_2$:xEu^{2+} (x = 0.01, 0.03, 0.05, 0.08 and 0.10) phosphors.

x(Eu^{2+})	(x, y)
0.01	(0.2169, 0.2543)
0.03	(0.2089, 0.2674)
0.05	(0.2172, 0.2790)
0.08	(0.2423, 0.2951)
0.10	(0.2639, 0.3097)

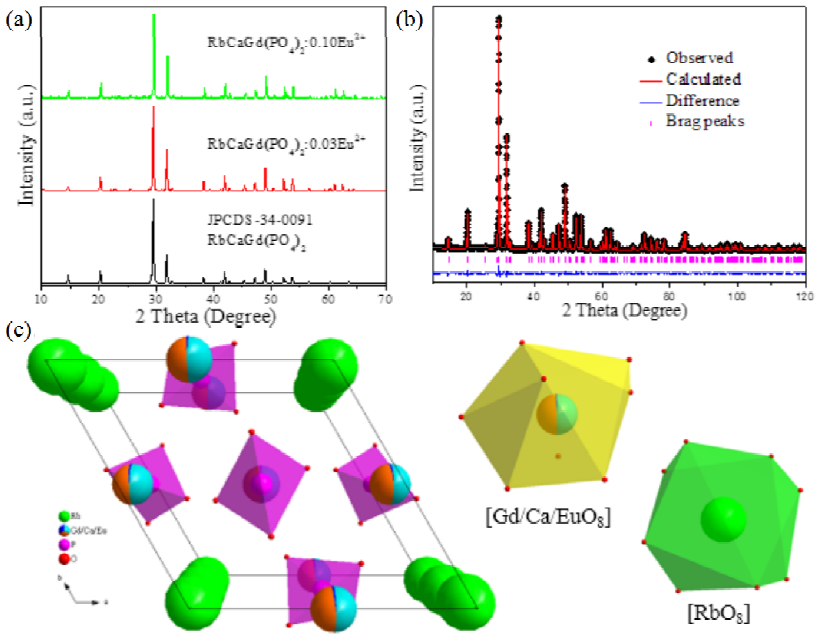

Figure 1 XRD patterns of the as-prepared $RbCaGd(PO_4)_2:Eu^{2+}$ phosphors (a), rietveld structure analysis (b) of the selected $RbCaGd(PO_4)_2:0.03Eu^{2+}$ phosphor and crystal structure (c) of $RbCaGd(PO_4)_2$.

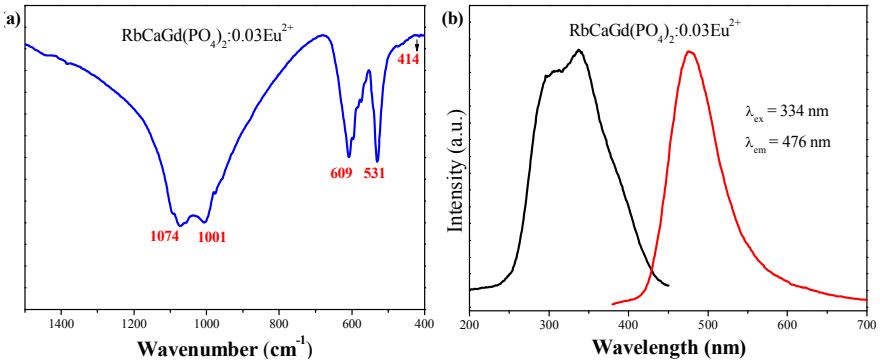

Figure 2 The FT-IR spectrum (a), PL and PLE spectra (b) of the $RbCaGd(PO_4)_2:0.03Eu^{2+}$ phosphor.

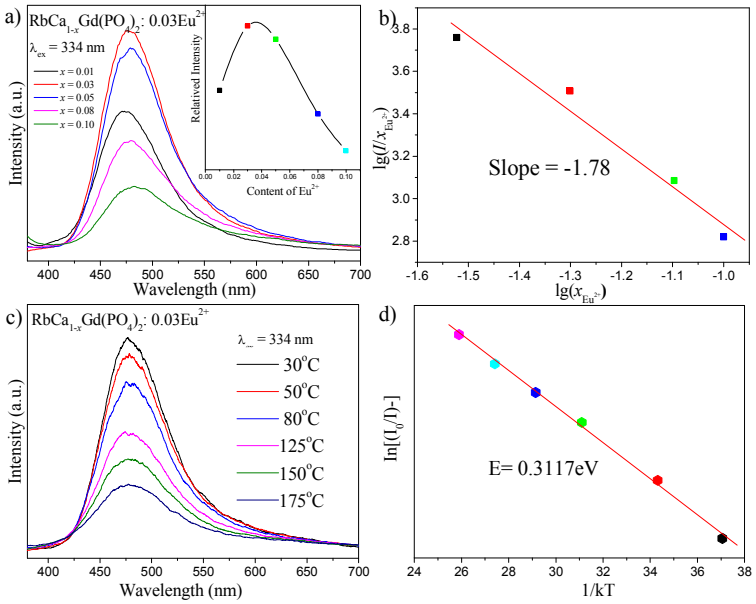

Figure 3 PL spectra (a) and relationship (b) of log(x) *vs*. log(I/x) for the $RbCaGd(PO_4)_2$:xEu^{2+} (x = 0.01, 0.03, 0.05, 0.08 and 0.10) phosphors, emission spectra (c) of $RbCaGd(PO_4)_2$:$0.03Eu^{2+}$ excitation under 334 nm at different temperature and (d) activation energy of thermal quenching.

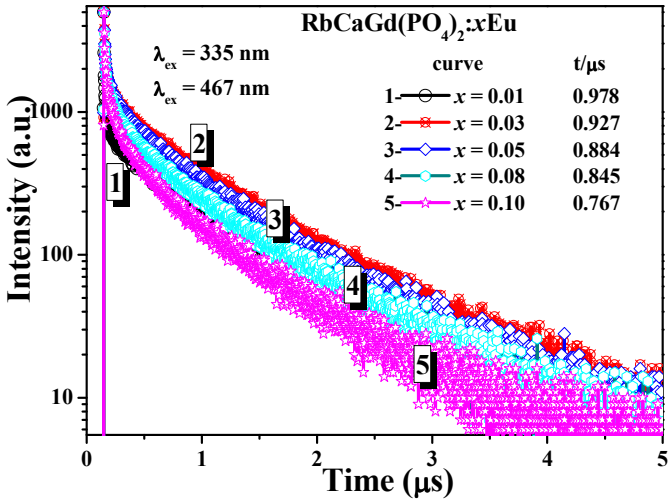

Figure 4 Decay curves of Eu^{2+} in $RbCaGd(PO_4)_2$:$x$$Eu^{2+}$ phosphors (excited at 335 nm, monitored at 467 nm).

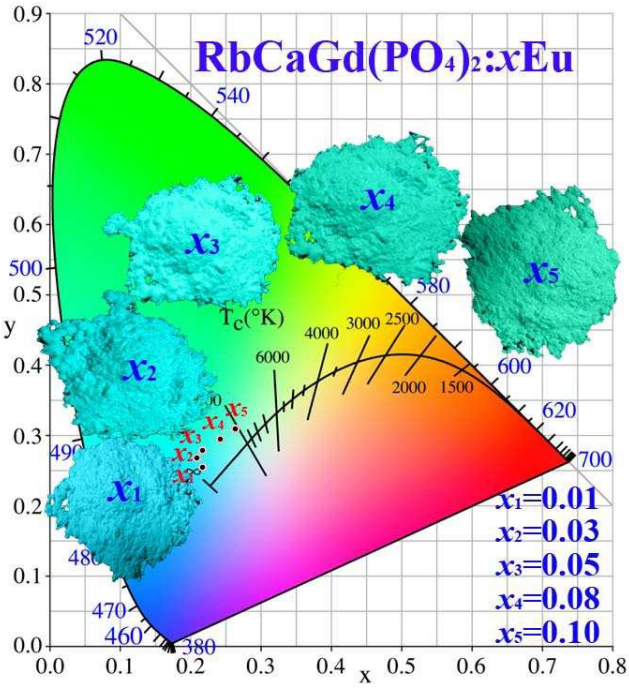

Figure 5 CIE chromaticity diagram and the digital photograph for $RbCaGd(PO_4)_2$:xEu^{2+} (x = 0.01, 0.03, 0.05, 0.08 and 0.10) excited by 365 nm.

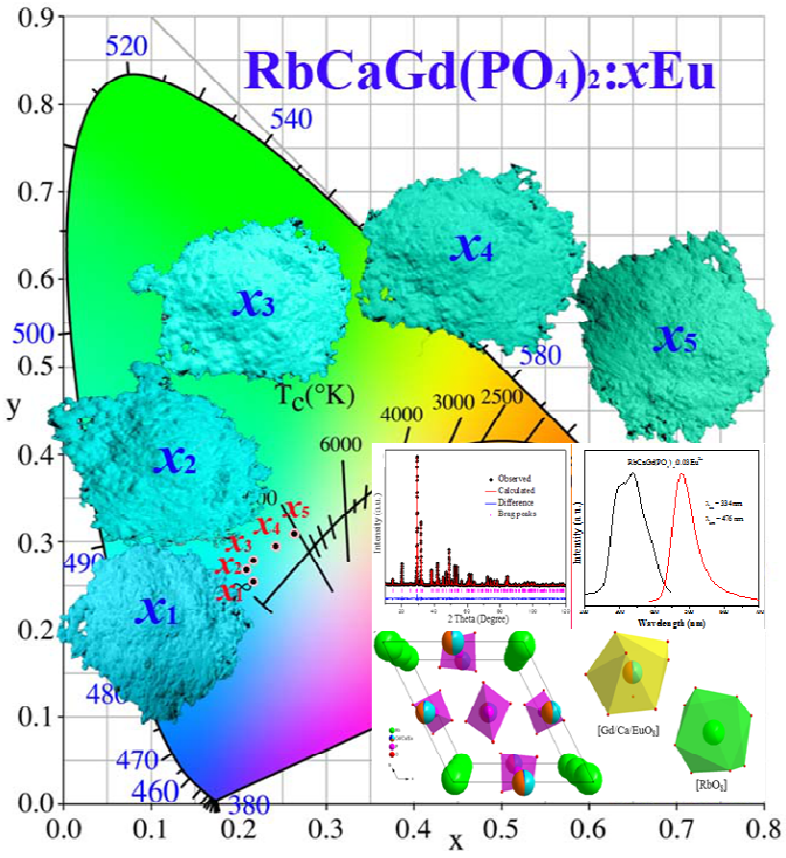

In this Letter, a novel double-phosphate phosphor, $RbCaGd(PO_4)_2:Eu^{2+}$, was prepared by the Pechini-type sol-gel method. The crystal structure was determined in the first time based on Rietveld refinements. Based on the experimental results and the theoretical calculation, it is identified that the dipole-dipole interaction plays a major role in the mechanism of concentration quenching of Eu^{2+} in this phosphor.